JPEDAV (2007) 28:130–138
DOI: 10.1007/s11669-006-9011-8
1547-7037 ©ASM International

Modeling of Microstructure and Microsegregation in Solidification of Multi-Component Alloys

M.-F. Zhu, W. Cao, S.-L. Chen, C.-P. Hong, and Y. A. Chang

(Submitted October 29, 2006)

Driven by industrial demand, extensive efforts have been made to investigate microstructure evolution and microsegregation development during solidification of multicomponent alloys. This paper briefly reviews the recent progress in modeling of microstructures and microsegregation in solidification of multicomponent alloys using various models including micromodel, phase field, front tracking, and cellular automaton approaches. A two-dimensional modified cellular automaton (MCA) model coupled with phase diagram software PanEngine is presented for the prediction of microstructures and microsegregation in the solidification of ternary alloys. The model adopts MCA technique to simulate dendritic growth. The thermodynamic data needed for determining the dynamics of dendritic growth are calculated with PanEngine. After validating the model by comparing the simulated values with the prediction of the Scheil model for solute profiles in the primary dendrites as a function of solid fraction, the model was applied to simulate the microstructure and microsegregation in the solidification of Al-rich ternary alloys. The simulation results demonstrate the capabilities of the present model not only to simulate realistic dendrite morphologies, but also to predict quantitatively the microsegregation profiles in the solidification of multi-component alloys.

Keywords cellular automaton, microsegregation, microstructure, modeling, multi-component alloys, PanEngine, solidification

1. Introduction

The microstructure and microsegregation that develop in solidification are of particular importance since they have a significant influence on the subsequent thermomechanical and heat treatment processing or the performance of as-cast materials. As most commercial materials are multi-component alloy systems and the analysis of solidification in multi-component alloys presents much greater difficulties than that in binary alloys, research on microstructure and microsegregation evolution in multi-component alloy solidification has received increasing interest not only from the fundamental point of view of understanding the origin of complex morphologies and related phenomena, but also from the practical point of view of recognizing microstructures closely associated with properties.[1]

Over the last decade, in parallel to the development of rigorous analytical models and refined experimental techniques, numerical modeling has emerged as a powerful and important tool to study the evolution of microstructure and microsegregation during solidification of alloys. Coupled with thermodynamics calculations, various numerical models[2-17] have been developed to describe the solidification process in multi-component alloys.

One-dimensional (1-D) microscopic models were first developed to analyze the microsegregation and solidification path in multi-component alloy systems.[2-5] In the models the dendrite morphology is usually assumed to be plate, cylinder, or sphere having a length scale of half the secondary dendrite arm spacing. In addition, diffusion in the liquid is considered to be complete and thus the liquid composition is essentially uniform. Xie et al.[2-4] developed a micromodel based on a modified Scheil model, which accounts for solid back diffusion, undercooling and dendrite arm coarsening, with dynamic coupling to the multi-component phase equilibrium calculation engine PanEngine.[18] The model was applied to investigate microsegregation in ternary and higher order alloys such as aluminum 7050 alloy containing 11 components and forming six different intermetallic phases in subsequent eutectic reactions during solidification. The predicted results of microsegregation compare well with the experimentally measured

This article was presented at the Multi-Component Alloy Thermodynamics Symposium sponsored by the Alloy Phase Committee of the joint EMPMD/SMD of The Minerals, Metals, and Materials Society (TMS), held in San Antonio, Texas, March 12-16, 2006, to honor the 2006 William Hume-Rothery Award recipient, Professor W. Alan Oates of the University of Salford, UK. The symposium was organized by Y. Austin Chang of the University of Wisconsin, Madison, WI, Patrice Turchi of the Lawrence Livermore National Laboratory, Livermore, CA, and Rainer Schmid-Fetzer of the Technische Universitat Clausthal, Clauthal-Zellerfeld, Germany.

M.-F. Zhu, School of Materials Science and Engineering, Southeast University, Nanjing 210096, China; **W. Cao** and **Y. A. Chang,** Department of Materials Science and Engineering, University of Wisconsin-Madison, 1509 University Avenue, Madison, WI; **S.-L. Chen,** CompuTherm LLC, 437 S. Yellowstone Dr., Suite 217, Madison, WI; and **C.-P. Hong,** Center for Computer-Aided Materials Processing (CAMP), Department of Metallurgical Engineering, Yonsei University, Shinchon-dong 134, Seodaemun-ku, Seoul 120-749, Korea. Contact e-mail: zhumf@seu.edu.cn

data. However, there are some limitations of 1-D models. For example, they cannot describe realistic microstructure formation, the effect of limited liquid diffusivity on the microsegregation, solute trapping, and other non-equilibrium phenomena in solidification of multi-component alloys.

On the other hand, various two-dimensional (2-D) and three-dimensional (3-D) microstructure models, such as Phase Field (PF), front tracking (FT), and cellular automaton (CA), are able to readily handle the complex microstructural evolution, which involves diffusion in both solid and liquid, coarsening of dendrites, the curvature, and kinetic effects on the moving solid/liquid (SL) interface. Thus, these approaches are expected to be more effective to describe realistic-looking microstructures with different phases forming at different locations in space as well as microsegregation maps.

The Phase-Field (PF) method is an elegant and integrated simulation technique for describing complex pattern evolution in phase transitions quantitatively. The PF models have recently been extended to multi-component alloy systems via coupling of the phase field equations to thermodynamic databases and equilibrium calculations. Ode et al.[6,7] have developed a PF model for ternary alloys to simulate isothermal dendrite growth and microsegregation in Fe-C-P and Al-Si-Mg alloys under different conditions of cooling rate and alloy composition. Grafe et al.[8] proposed a multi-component extension to a multi-Phase-Field model. The model was applied to simulate 2-D Ostwald-ripening of spherical γ' precipitates in a ternary Ni-Al-Cr alloy with a small γ-γ' lattice mismatch. The calculated and experimentally determined growth rates are of the same order of magnitude, indicating the feasibility of quantitative PF simulations of diffusion controlled phase transformations in technical multi-component alloys. The PF model has also been developed to study the solidification of multi-component alloys containing substitutional and interstitial solute elements.[9] Chen et al.[10] carried out quantitative simulations of diffusion-controlled precipitate growth and dissolution in Ti-Al-V alloys by applying a multi-component PF model that makes direct use of assessed thermodynamic and mobility databases. More recently, Böttger and Steinbach reported their work about the PF simulation of microstructure formation during multiphase solidification in multi-component alloys. Their approach is the online-coupling of CALPHAD-databases to the Phase-Field software MICRESS using the Thermo-Calc Fortran interface. The model has been applied to multi-component hypereutectic aluminum casting alloys, which exhibit a rather complex solidification sequence and microstructure.[11] As it is well-known that the most serious problem with the PF model is that it requires massive computer resources. This problem limits the use of PF technique to relatively large undercoolings and on small domains, for a few dendrites, or using simulation time in the order of weeks to months, even when adaptive grid methods or parallel techniques are adopted.[19]

Jacot and Rappaz have developed a pseudo-front tracking (PFT) model for the simulation of the primary phase formation during solidification of multi-component alloys.[12] The advantage of the PFT model is in allowing for simulations of primary phase formation under normal solidification conditions without the non-equilibrium effects present in PF modeling. The model was coupled with the phase diagram software Thermo-Calc to calculate the equilibrium concentrations at the SL interface. It was shown that the model is capable of reproducing various types of microstructures such as globular, globulo-dendritic, and dendritic grains in a ternary Al-1%Mg-1%Si alloy under different cooling and nucleation conditions. However, since the algorithm for reconstructing the interface from the solid fraction field involves complex numerical calculations, the PFT model also suffers from a very high computational cost, even two to four times more computationally intensive than the PF model.

The models based on the cellular automaton (CA) technique can reproduce a wide range of microstructure features observed experimentally with an acceptable computational efficiency, indicating its excellent potential for engineering applications. CA models have thus recently generated considerable interest and have led to advances in the modeling of microstructure evolution during solidification.[20-23] The progress in the CA models for the simulation of microstructures in solidification of binary alloys has recently reviewed by some of the present authors.[24] The CA models have also been extended to multi-component alloy systems. Jarvis et al.[13] have developed a cellular automaton-finite difference (CAFD) model to predict microsegregation patterns and the appearance of non-equilibrium constituents during non-equilibrium solidification of multi-component and multi-phase alloys. Simulations of a directionally-solidified Al-3.95Cu-0.8Mg alloy were performed and compared with experimental results, with respect to the amounts of non-equilibrium constituents and solute profiles in the primary α phase. The results show good agreement between all the 1-D, 2-D, and 3-D CAFD simulations. The simulated curves fall within the limits of the equilibrium and the Scheil profiles, but lie very close to the latter. However, discrepancies occur between the simulated and experimental distribution curves for copper in the primary α phase. Possible reasons attributed to the discrepancies between the simulations and the experiments were analyzed. Lee et al.[14] have developed a multiscale model, which spans almost six orders of magnitude in spatial phenomena, to simulate solidification microstructures and microporosity in an Al-Si-Cu alloy. At the microscale, a combined stochastic-deterministic approach, based on the CA method, is used to solve the multi-component diffusion equations in a three-phase system (liquid, solid, and gas), simulating the nucleation and growth of both grains and pores. The microscale model is coupled with a commercial finite element solver ProCAST to simulate the macroscopic heat transfer and fluid flow. The required thermodynamic data are calculated using Thermo-Calc. The model is capable of simulating the dendritic structure of the primary phase, together with the complex three dimensional shapes of the porosity.

In the present paper, a 2-D modified cellular automaton (MCA) model is extended to a multi-component alloy system by coupling with the thermodynamic and phase equilibrium calculation engine PanEngine.[18] The validity of the model is examined through comparison of the model calculations with the predictions of the Scheil model. Then the model is applied to simulate the evolution of

microstructure and microsegregation in Al-rich ternary alloys solidified under various cooling conditions.

2. Model Description and Numerical Algorithm

Two of the key thermodynamic parameters needed for the microstructural modeling of alloys are the solute partition coefficient and the liquidus slope. For simple binary model alloy systems, they are usually considered to be suitably taken as a constant. However, for multi-component systems, the actual values may vary significantly with temperature and compositions. Accordingly, it is necessary to couple the thermodynamic and phase equilibrium calculations in the modeling of microstructure and microsegregation for multicomponent alloys.

In the present work, a MCA approach for microstructure simulation is coupled with the sophisticated multi-component phase equilibrium calculation engine PanEngine to obtain phase equilibrium information for the ternary Al-Cu-Mg alloy systems. PanEngine, developed by CompuTherm LLC, is the core component of the phase diagram calculation software—PANDAT.[18] It is able to solve for the phase equilibrium when the liquid phase reaches the region where one or more solid phases form simultaneously. To reduce the computation time, the coupling strategy between the MCA and PanEngine is based on a data tabulation. Before starting the MCA microstructure simulation, a data file is generated by PanEngine, in which the equilibrium liquidus temperatures and the equilibrium solid compositions are tabulated with respect to the relevant liquid compositions for a uniform grid spacing of 1 at.%. During the MCA simulation, the required thermodynamic data of equilibrium liquidus temperature and interface solid compositions are interpolated from the data stored in the tabulation grid.

A two-dimensional (2-D) rectangular computation domain is divided into a uniform orthogonal arrangement of cells. Each cell is characterized by several variables, such as temperature, concentrations of two solutes, crystallographic orientation, solid fraction, etc., and identified as the state of liquid ($f_s = 0$), solid ($f_s = 1$), or interface ($0 \leq f_s$). Since nucleation is not addressed in the present work, at the beginning of simulation, several isolated crystal seeds with different preferential growth orientations are randomly assigned in the domain which is initially at a homogeneous temperature and composition. The seeds are given an index indicating their preferred crystallographic orientation of θ_0 with respect to the horizontal direction.

Since the heat diffusivity is several orders of magnitudes larger than the solute diffusivity, thermal diffusion can be considered to be complete at the microscopic level and the kinetics for microstructure evolution during alloy solidification is assumed to be controlled by solute transport. Therefore, for the sake of simplicity, the thermal field in the domain is assumed as uniform and cooled down from the liquidus with an imposed cooling rare. It is known that for Al-rich ternary alloys, the solidification sequence is primary α phase $\rightarrow$ (eutectic like phase) $\rightarrow$ ternary eutectic. However, in the present work, we only consider primary α dendrites solidified from melt liquid. Thus, the simulation ends when the temperature is down to the point just before where binary eutectic formation commences.

To describe phase transformations in a ternary alloy system, two solute fields must be calculated. It is assumed that there is no convection in the melt and that solute transport is purely diffusive. The governing equation for solute diffusion within the entire domain is given by

$$\frac{\partial C_i(m)}{\partial t} = \nabla \cdot [D_i(m) \nabla C_i(m)] \quad (i = s, l \text{ and } m = 1, 2) \tag{Eq 1}$$

where $C_i(m)$ is the concentration and $D_i(m)$ is the diffusion coefficient of solute element (m) in phase (i). All diffusion coefficients $D_i(m)$ are considered to be independent of composition but temperature dependent. Two solutes are considered to diffuse independently of each other and cross diffusion is neglected. Within the interface region, the solid and the liquid phases are assumed to be in equilibrium and thus solute diffusion between the liquid and solid phases is ignored. Equation (1) is solved using an explicit finite difference scheme. The zero-flux boundary condition is applied for the cells located at the four walls of the calculation domain.

The growth of the dendrite is driven by the local undercooling. The local undercooling at time t_n, $\Delta T(t_n)$, is considered to be the difference between the local equilibrium liquidus temperature and the local actual temperature, incorporating the effect of curvature and it is represented by

$$\Delta T(t_n) = T^*(t_n) - T(t_n) - \Gamma(\theta)\bar{K}(t_n) \tag{Eq 2}$$

where $T^*(t_n)$ is the local equilibrium liquidus temperature and $T(t_n)$ is the local actual temperature which is determined by the imposed cooling rate. $\Gamma(\theta)$ is the Gibbs-Thomson coefficient. The local interface curvature, $\bar{K}(t_n)$, is calculated using the following equation[23]

$$\bar{K}(t_n) = \left[\left(\frac{\partial f_s}{\partial x}\right)^2 + \left(\frac{\partial f_s}{\partial y}\right)^2\right]^{-3/2} \left[2\frac{\partial f_s}{\partial x}\frac{\partial f_s}{\partial y}\frac{\partial^2 f_s}{\partial x \partial y} - \left(\frac{\partial f_s}{\partial x}\right)^2\frac{\partial^2 f_s}{\partial y^2} - \left(\frac{\partial f_s}{\partial y}\right)^2\frac{\partial^2 f_s}{\partial x^2}\right] \tag{Eq 3}$$

The growth velocity V_g and local undercooling is related by the classical sharp interface model[25]

$$V_g = \mu_k(\theta) \cdot \Delta T(t_n), \tag{Eq 4}$$

where $\mu_k(\theta)$ is the interface kinetic coefficient.

It is well-known that dendrites always grow in specific crystallographic orientations. Therefore, it is necessary to consider anisotropy in either the surface energy or interfacial attachment kinetics (or both) in the models of dendritic growth.[26] The present model accounts for the anisotropy in both surface energy and interfacial kinetics. For a fcc-lattice crystal of Al-rich Al-Cu-Mg alloys used in the present simulations, a 4-fold anisotropy of the surface energy and kinetics at the SL interface is exhibited. The Gibbs-Thomson coefficient $\Gamma(\theta)$ and the interface kinetics coefficient $\mu_k(\theta)$ are thus given by

$$\Gamma(\theta) = \bar{\Gamma}\{1 - \delta_t \cos[4(\theta - \theta_0)]\} \quad \text{(Eq 5)}$$

$$\mu_k(\theta) = \bar{\mu}_k\{1 + \delta_k \cos[4(\theta - \theta_0)]\}, \quad \text{(Eq 6)}$$

where $\bar{\mu}_k$, δ_k, $\bar{\Gamma}$, and δ_t are the average interface kinetic coefficient, the degree of the kinetic anisotropy, the average Gibbs-Thomson coefficient, and the degree of the surface energy anisotropy, respectively. θ is the angle between the normal of the SL interface and the horizontal direction, and θ_0 is the preferred growth orientation of the crystal. The angle θ can be calculated according to the gradient of solid fraction at the SL interface using the following equation

$$\theta = \arctan\left(\frac{\partial f_s}{\partial y}\Big/\frac{\partial f_s}{\partial x}\right) \quad \text{(Eq 7)}$$

The growth velocities of interface cells were calculated with Eq 2 through 7. The change in the rate of the solid fraction in an interface cell can thus be evaluated from the crystal growth velocity V_g as follows

$$\frac{\partial f_s}{\partial t} = G\frac{V_g}{\Delta x} \quad \text{(Eq 8)}$$

where Δx is the cell spacing. G is a geometrical factor related to the state of neighbor cells, which is defined by

$$G = \min\left[1, \frac{1}{2}\left(\sum_{m=1}^{4} s_m^I + \frac{1}{\sqrt{2}}\sum_{m=1}^{4} s_m^{II}\right)\right] \quad \text{(Eq 9)}$$

where s^I and s^{II} indicate the state of the nearest neighbor cells and the second-nearest neighbor cells, respectively. According to the state of a neighbor cell, s^I and s^{II} are determined by

$$s^I, s^{II} = \begin{cases} 0 & (f_s < 1) \\ 1 & (f_s = 1) \end{cases} \quad \text{(Eq 10)}$$

It is assumed that the thermodynamical local equilibrium is maintained at the SL interface and thus the solidified cells always adopt the equilibrium solid composition. As the dendrite grows, the growing cells reject solutes at the SL interface. The rejected amount of solute element (m) is evaluated by

$$\Delta C(m) = \Delta f_s\left(C_l^*(m) - C_s^*(m)\right) \quad \text{(Eq 11)}$$

where Δf_s is the solid fraction increment of an interface cell at one time step, which is evaluated by Eq 8. $C_l^*(m)$ and $C_s^*(m)$ are the interface liquid and solid compositions of solute element (m), respectively. The rejected $\Delta C(m)$ is added to the remaining liquid in the same cell and its surrounding neighbor cells. Thus, the overall amounts of solutes in the domain can be kept constant. The interface solid composition, $C_s^*(m)$, in Eq 11 and interface equilibrium liquidus temperature, $T^*(t_n)$, in Eq 2 are obtained by interpolation according to the local interface liquid compositions of two solutes, $C_l^*(1)$ and $C_l^*(2)$, which are determined by numerically solving Eq 1. The physical parameters used in the present work are given in Table 1.

3. Results and Discussion

According to Eq 4, after numerically calculating the local SL interface undercooling $\Delta T(t_n)$, the interface kinetic coefficient $\mu_k(\theta)$ is necessary for calculating the interface growth velocity. In the present work, the average interface kinetic coefficient $\bar{\mu}_k$ for Al-rich Al-Cu-Mg ternary alloys is determined by comparing the solid fraction evolution with temperature predicted by the Scheil model. The simulation was performed with the conditions of zero solid diffusivity and complete mixing in the liquid, which are exactly identical with the Scheil assumptions. The calculated solid fraction evolution as a function of decreasing temperature was recorded and compared with the Scheil prediction. The Scheil profile was calculated using PANDAT. Figure 1 indicates the comparison between the Scheil data and MCA model calculation with $\bar{\mu}_k = 3.0 \times 10^{-4}$ m/(sK) for an Al-3.9 wt.%Cu-0.9 wt.%Mg alloy. It is noted that the calculated data coincide very well with the Scheil profile. Therefore, in the present work, the average interface kinetic coefficient $\bar{\mu}_k$ is taken as 3.0×10^{-4} m/(sK).

In order to validate the MCA model for the prediction of microsegregation in ternary alloy solidification, the simulated solid composition profiles of two solutes for an Al-3.9 wt.%Cu-0.9 wt.%Mg alloy by the present model with assumptions of zero solid diffusivity and complete liquid mixing are compared with the Scheil predictions. The agreements are well observed as shown in Fig. 2.

The MCA model is then applied to the simulation of the microstructure and microsegregation in ternary alloy solidification with the realistic diffusivities. Figure 3 shows the simulated dendrite morphology and composition fields of two solutes copper and magnesium for an Al-15 wt.%Cu-

Table 1 Physical parameters used in the present work

Symbol	Definition and unites	Value	References
D_l (Cu)	Liquid diffusion coefficient of Cu, m^2/s	$1.05 \times 10^{-7}\exp(-2856/T)$	3,12
D_s (Cu)	Solid diffusion coefficient of Cu, m^2/s	$2.9 \times 10^{-5}\exp(-15600/T)$	12
D_l (Mg)	Liquid diffusion coefficient of Mg, m^2/s	$9.9 \times 10^{-5}\exp(-8610/T)$	3,12
D_s (Mg)	Solid diffusion coefficient of Mg, m^2/s	$0.37 \times 10^{-4}\exp(-14854/T)$	6
δ_k	Degree of kinetic anisotropy	0.3	27
δ_t	Degree of surface energy anisotropy	0.3	27
$\bar{\Gamma}$	Average Gibbs-Thomson coefficient, mK	1.7×10^{-7}	27

1 wt.%Mg alloy with a cooling rate of 10 °C/s when the temperature is cooled down to the binary eutectic temperature of 537 °C. The simulations were performed in a domain consisting of 230 × 230 cells with a cell size of 2 μm. It can be noted from Fig. 3 that the dendrite morphology of this alloy exhibits well developed side branches. Since the simulation stopped at the end of primary α dendrite solidification, the light gray in Fig. 3(a) and black color in Fig. 3(b) indicate the remaining interdendritic liquid that will transform to binary and ternary eutectics in the subsequent solidification. The calculation time for simulating Fig. 3 is only about half hour on a PC Pentium IV with CPU-2.4 GHz, indicating an excellent computational efficiency of the present model.

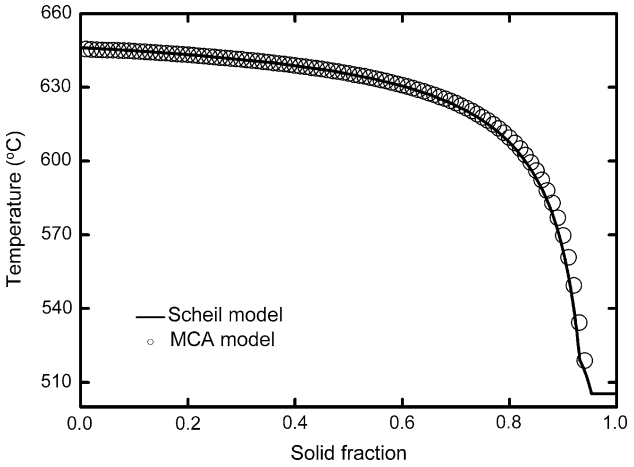

Fig. 1 Solid fraction evolution with temperature for an Al-3.9 wt.%Cu-0.9 wt.%Mg alloy—comparison between the Scheil prediction and MCA calculation with the condition of zero solid diffusivity and complete liquid mixing

During the primary dendritic solidification, the liquid composition increases because of the solute partition at the SL interface, leading to a continuous increase in solid composition of the newly-formed solid. The variation of solid composition with the increase of solid fraction obtained from the model calculation was measured and recorded for comparison with the predictions of the Scheil model. As mentioned previously, the MCA simulation involves non-zero solid diffusivity and limited liquid diffusivity using the realistic solute diffusivities, whereas the Scheil model is derived based on the assumptions of no diffusion in the solid and complete mixing in the liquid. To analyze the effects of diffusion in the liquid and solid on microsegregation, respectively, comparison with the Scheil model was made in two steps. As the first step, the simulations were carried out with the condition of zero solid

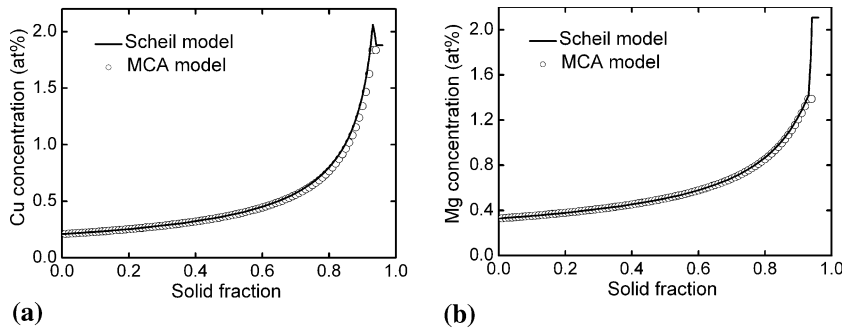

Fig. 2 Comparison between the Scheil model and the present MCA model with zero solid diffusivity and complete liquid mixing for predicting solute concentration profiles of (a) Cu; and (b) Mg as a function of solid fraction for an Al-3.9 wt.%Cu-0.9 wt.%Mg alloy

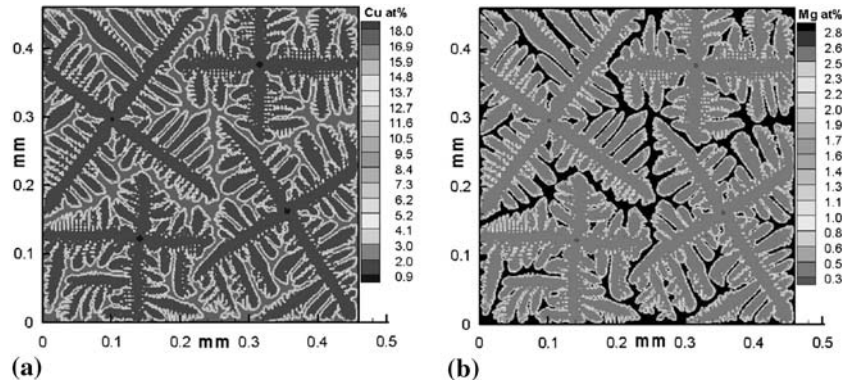

Fig. 3 Simulated equiaxed dendrite morphology and solute fields of (a) Cu; and (b) Mg for an Al-15 wt.%Cu-1 wt.%Mg alloy solidified with 10 °C/s

diffusivity ($D_s(m) = 0$) and finite liquid diffusivity ($D_l(m) > 0$). The simulated solid composition profiles of two solutes with the cooling rates of 0.25, 10, and 100 °C/s are compared with the Scheil predictions in Fig. 4. It can be noted that the solid compositions of both solutes Cu and Mg predicted by the Scheil model are relatively lower at the early solidification stage but higher at the later stages. On lowering the solidification rate, the difference between the simulated data and the Scheil profiles decreases. In case of very low cooling rate of 0.25 °C/s, the MCA calculated data are nearly superposed on the Scheil profiles.

Figure 5 indicates the simulated dendritic morphologies and Cu composition fields with various cooling rates of 0.25, 10, and 100 °C/s when the total solid fraction is 0.2. It can be noted from Fig. 5(a) that for the case of 0.25 °C/s cooling rate, enough time is available for solute diffusion in the liquid, resulting in an almost uniform liquid composition field which is very close to the Scheil condition. However, with an increase in cooling rate, solute gets amassed in front of the SL interface, which not only enhances the interface instability to cause side branches, but also results in solute trapping in the early solidified region, and thus a relatively lower composition is produced in the late solidified region. The higher the cooling rate, the heavier the solute buildup in front of the SL interface as shown in Fig. 5(b), (c). Similar results were observed for the solute Mg. Consequently, it is understandable that the difference between the simulated data and the Scheil profiles increases with solidification rate as is indicated in Fig. 4.

The second step is to investigate the effect of solid diffusion on the solute microsegregation. The simulations were performed with zero and non-zero solid diffusivity for the cooling rates of 0.25 and 20 °C/s, respectively. A finite liquid diffusivity ($D_l(m) > 0$) was adopted for all simulations. The results are presented in Fig. 6 and 7. It can be seen from Fig. 6 that for the case of 20 °C/s cooling rate, two sets of data calculated from zero and non-zero solid diffusivity are almost superposed for both solutes Cu and Mg. Since in this case the total solidification time is only about 4 s, it is not long enough to generate any detectable back diffusion. On the other hand, when the cooling rate slows down to 0.25 °C/s, the composition profiles of both Cu and Mg solutes with non-zero solid diffusivities are higher at the early stage and lower later than those obtained with zero solid diffusivity, indicating the evident effect of back diffusion. This is understandable, in that the slow solidification process provides a longer time for solid diffusion. In addition, comparing two solutes, Mg exhibits a more obvious back diffusion effect, since the solid diffusion coefficient of Mg is larger than that of Cu. Accordingly, the present model not only allows reproducing realistic-looking multi-dendritic morphologies, but also predicts reasonably well the microsegregation patterns depending on the involved solidification conditions.

The model was also applied to simulate the formation of multi-equiaxed dendrites in an Al-3.9 wt.%Cu-0.9 wt.%Mg alloy.[28] The simulation was carried out in a domain consisting of 300 × 300 cells with a cell size of 3 μm.

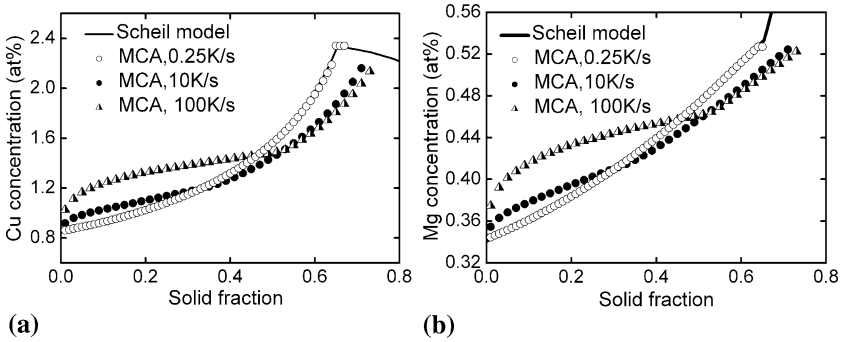

Fig. 4 Comparison between the Scheil model and the MCA model for predicting solute concentration profiles of (a) Cu; and (b) Mg as a function of solid fraction for an Al-15 wt.%Cu-1 wt.%Mg alloy with various solidification rates

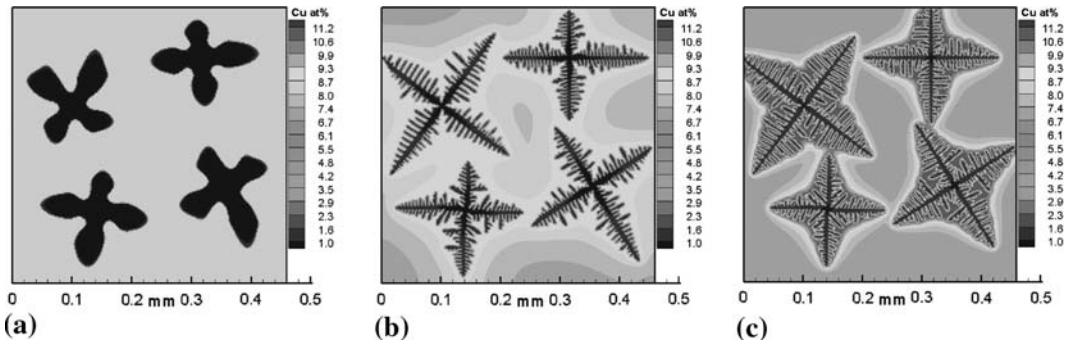

Fig. 5 Simulated dendritic morphologies and Cu composition fields for an Al-15 wt.%Cu-1 wt.%Mg alloy (f_s = 0.2) with various solidification rates of (a) 0.25 °C/s; (b) 10 °C/s; and (c) 100 °C/s

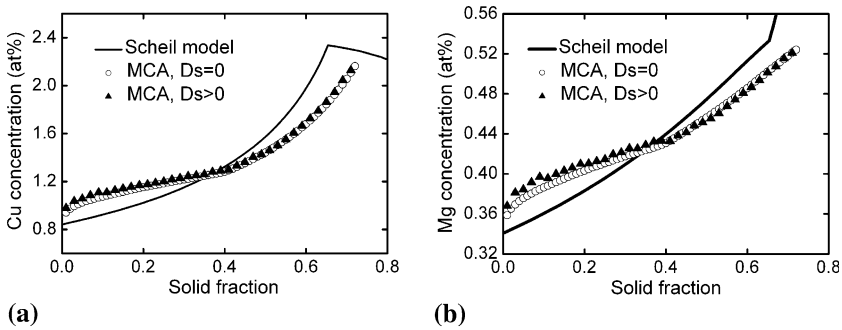

Fig. 6 Predicted concentration profiles of (a) Cu; and (b) Mg as a function of the solid fraction for an Al-15 wt.%Cu-1 wt.%Mg alloy solidified with 20 °C/s

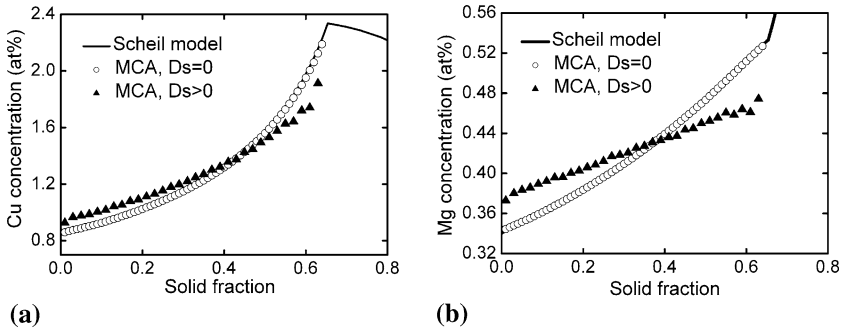

Fig. 7 Predicted concentration profiles of (a) Cu; and (b) Mg as a function of the solid fraction for an Al-15 wt.%Cu-1 wt.%Mg alloy solidified with 0.25 °C/s

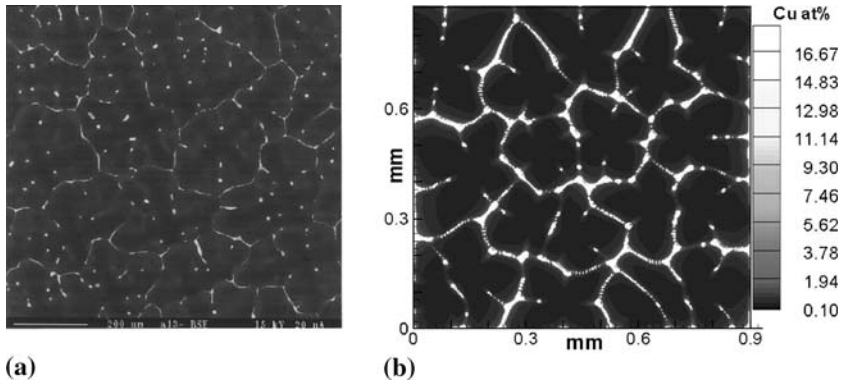

Fig. 8 Dendrite morphology of an Al-3.9 wt.%Cu-0.9 wt.%Mg alloy solidified with 0.78 °C/s: (a) experiment;[2] and (b) simulation

Several nuclei having the randomly assigned preferred growth orientations θ_0 ranging from 0° to 90° with respect to the horizontal direction were randomly distributed on the domain. The temperature of the domain was assumed to be uniform and cooled down from the liquidus temperature of 646 ° C to the binary eutectic temperature of 519 °C with a constant cooling rate of 0.78 °C/s. Figure 8 shows a comparison between the experimental microstructure and the simulated dendritic morphology presented in the form of Cu solute map. An experimental microstructure shows the morphology in a transverse section of a directionally solidified Al-3.9 wt.%Cu-0.9 wt.%Mg alloy with 0.78 °C/s.[2] It can be noted from Fig. 8(b) that the outside shell of dendrites exhibits the higher composition. The white color along the grain boundaries indicates the remaining liquid at the end of primary αdendrite formation, which will transform to binary and ternary eutectics at the end of solidification.

4. Conclusions

An MCA model has been coupled with the thermodynamic and phase equilibrium calculation package PanEn-

gine for simulating the evolution of microstructure and microsegregation in a ternary alloy system. The model includes time-dependent calculations for the solute redistribution in the liquid and solid phases, interface curvature, and preferred crystallographic orientations. The evolution of the SL interface is considered to be driven by the difference between the local equilibrium liquidus temperature and the local actual temperature, incorporating the effect of curvature. Based on the interface liquid compositions of two solutes, which are determined by numerically solving the mass transport equation of two solutes in the whole domain, the local equilibrium liquidus temperature and interface equilibrium solid compositions of two solutes are obtained with the aid of PanEngine. The simulated composition profiles of two solutes as a function of solid fraction were compared with the predictions of the Scheil model for an Al-15 wt.%Cu-1 wt.%Mg alloy. The results show that the simulated solid compositions with the zero solid diffusivity and the finite liquid diffusivity were higher than the Scheil predictions in the early solidification stages and lower in the later stages, respectively. On lowering the cooling rates, the simulated solid composition profiles were found to be increasingly close to the Scheil profile. Moreover, at lower solidification rates, the calculated solid composition profiles with a non-zero solid diffusivity are initially higher and later lower than those obtained with a zero solid diffusivity, illustrating the effect of back diffusion. However, the effect of back diffusion is not evident when the solidification rate is increased. These simulation results demonstrate that the present model can predict reasonably well the microsegregation patterns in the solidification of ternary alloys depending on the cooling rate conditions involved. The model is also able to reproduce a realistic dendritic growth morphology which compares well with the experimental observations.

Acknowledgments

The research of M.F.Z. was supported by the National Natural Science Foundation of China under Grant Nos. 50371015 and 50671025. Y. Austin Chang wishes to thank NSF through the FRG Grant No. DMR-0309468 and Wisconsin Distinguished Professorship for support.

References

1. U. Hecht, L. Granasy, T. Pusztai, B. Bottger, M. Apel, V. Witusiewicz, L. Ratke, J. De Wilde, L. Froyen, D. Camel, B. Drevet, G. Faivre, S.G. Fries, B. Legendre, and S. Rex, Multiphase Solidification in Multicomponent Alloys, *Mater. Sci. Eng.*, 2004, **R46**, p 1-49, in English
2. F.-Y. Xie, T. Kraft, Y. Zuo, C.-H. Moon, and Y.A. Chang, Microstructure and Microsegregation in Al-rich Al-Cu-Mg Alloys, *Acta Mater.*, 1999, **47**, p 489-500, in English
3. X. Yan, S. Chen, F. Xie, and Y.A. Chang, Computational and Experimental Investigation of Microsegregation in an Al-rich Al-Cu-Mg-Si Quaternary Alloy, *Acta Mater.*, 2002, **50**, p 2199-2207, in English
4. F. Xie, X. Yan, L. Ding, F. Zhang, S. Chen, M.G. Chu, and Y.A. Chang, A Study of Microstructure and Microsegregation of Aluminum 7050 alloy, *Mater. Sci. Eng. A*, 2003, **355**, p 144-153, in English
5. K. Ohsasa, S. Nakaue, M. Kudoh, and T. Narita, Analysis of Solidification Path of Fe-Cr-Ni Ternary Alloy, *ISIJ Int.*, 1995, **35** (6), p 629-636, in English
6. M. Ode, J.S. Lee, S.G. Kim, W.T. Kim, and T. Suzuki, Phase-field Model for Solidification of Ternary Alloys, *ISIJ Int.*, 2000, **40** (9), p 870-876, in English
7. H. Kobayashi, M. Ode, S.G. Kim, W.T. Kim, and T. Suzuki, Phase-field Model for Solidification of Ternary Alloys Coupled with Thermodynamic Database, *Scripta Mater.*, 2003, **48**, p 689-694, in English
8. U. Grafe, B. Bottger, J. Tiaden, and S.G. Fries, Coupling of Multicomponent Thermodynamic Databases to a Phase Field Model: Application to Solidification and Solid State Transformations of Superalloys, *Scripta mater.*, 2000, **42**, p 1179-1186, in English
9. P.-R. Cha, D.-H. Yeon, and J.-K. Yoon, A Phase Field Model for Isothermal Solidification of Multicomponent Alloys, *Acta mater.*, 2001, **49**, p 3295-3307, in English
10. Q. Chen, N. Ma, K. Wu, and Y. Wang, Quantitative Phase Field Modeling of Diffusion-controlled Precipitate Growth and Dissolution in Ti-Al-V, *Scripta Mater.*, 2004, **50**, p 471-476, in English
11. B. Böttger and I. Steinbach, Online-Coupling of Thermodynamic Databases to a Multi-Phase-Field Model – Application to Hypereutectic Aluminum Casting Alloys, *TMS Annual Meeting*, February 13-17, 2005 (San Francisco, CA)
12. A. Jacot and M. Rappaz, A Pseudo-front Tracking Technique for the Modeling of Solidification Microstructures in Multicomponent Alloys, *Acta Mater.*, 2002, **50**, p 1909-1926, in English
13. D.J. Jarvis, S.G.R. Brown, and J.A. Spittle, Modeling of Non-equilibrium Solidification in Ternary Alloys: Comparison of 1D, 2D, and 3D Cellular Automaton-finite Difference Simulations, *Mater. Sci. Tech.*, 2000, **16**, p 1420-1424, in English
14. P.D. Lee, A. Chirazi, R.C. Atwood, and W. Wang, Multiscale Modelling of Solidification Microstructures, Including Microsegregation and Microporosity, in an Al-Si-Cu Alloy, *Mater. Sci. Eng. A*, 2004, **365**, p 57-65, in English
15. J. Miettinen, Thermodynamic-kinetic Simulation of Constrained Dendrite Growth in Steels, *Metall. Mater. Trans. B*, 2000, **31B**, p 365-379, in English
16. B. Bottger, U. Grafe, D. Ma, and S.G. Fries, Simulation of Microsegregation and Microstructural Evolution in Directionally Solidified Superalloys, *Mater. Sci. Tech.*, 2000, **16**, p 1425-1428, in English
17. B.J. Yang, D.M. Stefanescu, and J. Leon-Torres, Modeling of Microstructural Evolution with Tracking of Equiaxed Grain Movement for Multicomponent Al-Si Alloy, *Metall. Mater. Trans. A*, 2001, **32**, p 3065-3076, in English
18. S.-L. Chen, S. Daniel, F. Zhang, Y.A. Chang, X.-Y. Yan, F.-Y. Xie, R. Schmid-Fetzer, and W.A. Oates, The PANDAT Software Package and its Applications, *CALPHAD*, 2002, **26** (2), p 175-188, in English
19. J.A. Warren, I. Loginova, L. Granasy, T. Borzsonyi, and T. Pusztai, Phase Field Modeling of Alloy Polycrystals, *Modeling of Casting, Welding and Advanced Solidification Processes X*, D.M. Stefanescu, J. Warren, M. Jolly, and M. Krane, Ed., TMS Publication, Florida, May 25-30, 2003, p 45-52
20. L. Nastac, Numerical Modeling of Solidification Morphologies and Segregation Patterns in Cast Dendritic Alloys, *Acta Mater.*, 1999, **47**, p 4253-4262, in English

21. M.F. Zhu and C.P. Hong, A Modified Cellular Automaton Model for the Simulation of Dendritic Growth in Solidification of Alloys, *ISIJ Int.*, 2001, **41**, p 436-445, in English
22. W. Wang, P.D. Lee, and M. Mclean, A Model of Solidification Microstructures in Nickel-based Superalloys: Predicting Primary Dendrite Spacing Selection, *Acta Mater.*, 2003, **51**, p 2971-2987, in English
23. L. Belteran-Sanchez and D.M. Stefanescu, A Quantitative Dendrite Growth Model and Analysis of Stability Concepts, *Metall. Mater. Trans. A*, 2004, **35**, p 2471-2485, in English
24. M.F. Zhu, C.P. Hong, D.M. Stefanescu, and Y.A. Chang, Advances in Computational Modeling of Microstructure Evolution in Solidification of Aluminum Alloys, *Proceedings of Simulation of Aluminum Shape Casting Processing*, Q.G. Wang, M.J.M. Krane, and P.D. Lee, Ed., March 12-16, 2006 (San Antonio, TX) TMS 2006 Annual Meeting, TMS Publication, 2006, p 13-22, in English
25. A.A. Wheeler, W.J. Boettinger, and G.B. McFadden, Phase-field Model for Isothermal Phase Transitions in Binary Alloys, *Phys. Rev. A*, 1992, **45**, p 7424-7439, in English
26. L. Granasy, T. Pusztai, J.A. Warren, J.F. Douglas, T. Borzsonyi, and V. Ferreiro, Growth of 'Dizzy Dendrites' in a Random Field of Foreign Particles, *Nature Mater.*, 2003, **2**, p 92-96, in English
27. M.F. Zhu, S.Y. Lee, C.P. Hong, Modified Cellular Automaton Model for the Prediction of Dendritic Growth with Melt Convection, *Phys. Rev. E*, 2004, **69**, article No. 061610, in English
28. M.-F. Zhu, W.-S. Cao, S.-L. Chen, F.-Y. Xie, C.-P. Hong, and Y.A. Chang, Modified Cellular Automaton Model for Modeling of Microstructure and Microsegregation in Solidification of Ternary Alloys, *Trans. Nonferrous Met. Soc. China*, 2006, **16** (Special issue 2), p s180-s185, in English